Supporting Information

High-Sensitive Organic Quasi-tandem Narrowband Photodetector with Enhanced Spectral Selectivity

Yaqian Li, Jiaqi Shao, Yu Zhang, Ying Xu, Ziqi Zhu, Xiaowei Li, Zhiqin Liang, Bo Qiao, Dandan Song, Guangcai Yuan, Suling Zhao**

Corresponding author: Guangcai Yuan, Suling Zhao.
Email: yuanguangcai@boe.com.cn; slzhao@bjtu.edu.cn

Text S1

The distribution of photogenerated excitons within PM6 layers.

The one-dimensional continuity equation governing the density of photogenerated excitons $n(x, t)$ in the PM6 layer is as follows:

$$\frac{\partial n(x,t)}{\partial t} = gaN_0 e^{-\alpha x} - \frac{n(x,t)}{t} + D\frac{\partial^2 n(x,t)}{\partial^2 x} - F(x - x_{int})n(x,t) \#(S1)$$

The first term represents exciton generation, where photons are converted into excitons with an efficiency of g.a is the material's absorption coefficient, x is the penetration depth of incident light, and N_0 is the number of incident photons. The second term represents the exciton recombination with a recombination lifetime of t. The third term represents the exciton diffusion, where D is the exciton diffusion coefficient. The last term represents the exciton dissociation at the donor-acceptor interface (x_{int}), with a dissociation rate of $F(x - x_{int})$. Under equilibrium and boundary conditions, which satisfies $\partial n(x,t)/t = 0$, $n(x = 0) = 0$, and $n(x \to \infty) = 0$, the following solution can be derived[1]:

$$n(x) = \frac{gN_0}{D}\frac{\alpha L^2}{1 - (\alpha L^2)}\left(e^{-\alpha x} - e^{-\left(\frac{x}{L}\right)}\right) \#(S2)$$

where $L = \sqrt{Dt}$ is defined as the diffusion length of excitons. Equation S2 provides the distribution of exciton density in the front PM6 layer[2]. According to literature reports[3], the exciton diffusion length in PM6 thin films is 8.22 nm. Using the formula, we obtained the exciton density distribution curves for incident light of different wavelengths in the PM6 layer (Figure 1e).

Text S2

The specific detectivity D^* reflected the sensitivity of weak light detection can be calculated by[4]:

$$D^*(\lambda) = \frac{A^{1/2}}{NEP(\lambda)} \#(S3)$$

Where the *NEP* represent the noise equivalent power. The dark current (i_{dark}) is often considered a major factor affecting the noise current, so when the i_{dark} induces shot noise is the dominant factor, the shot noise limited D* can be calculated by[5, 6]:

$$D^*(\lambda) = D^*_{sh}(\lambda) = \frac{R(\lambda)}{\sqrt{2qJ_d}} \#(S4)$$

Where R is the responsivity, q is the elementary charge and J_d is the dark current density.

Text S3

The net photocurrent density (J_{ph}) is determined by calculating the difference between illuminated current density and dark current density. The effective voltage (V_{eff}) represents the difference

between applied voltage and built-in potential. With increasing V_{eff}, J_{ph} gradually reaches saturation, where the corresponding value is defined as the saturation photocurrent density ($J_{ph,sat}$). This saturation behavior indicates complete dissociation of photogenerated excitons under high applied voltage.

The charge transfer efficiency (P) under short-circuit conditions can be quantified using the following equation:

$$P = \frac{J_{ph-sc}}{J_{ph,sat}} \#(S4)$$

where $J_{ph\text{-}sc}$ denotes the photocurrent density under short-circuit conditions. A higher P value indicates more efficient charge collection within the device.

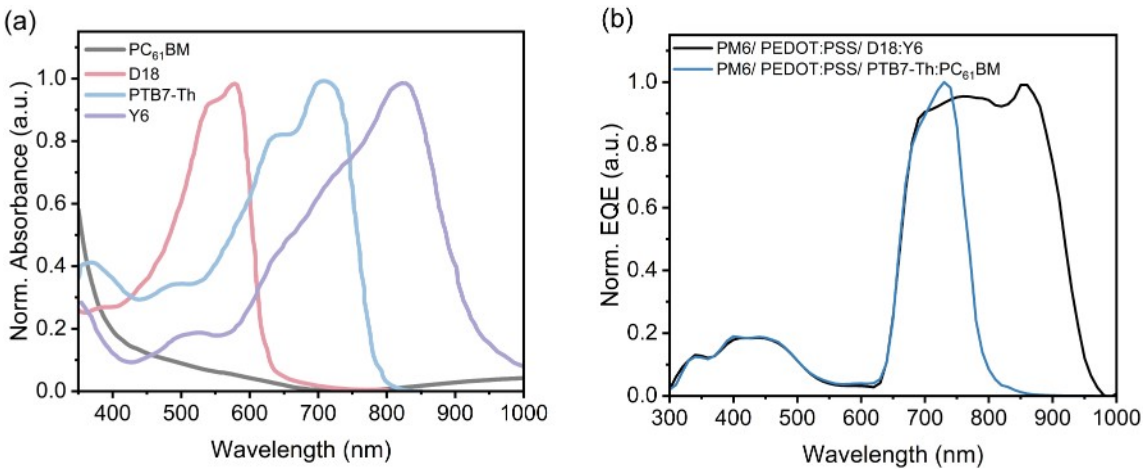

Figure S1. (a) The normalized absorption spectra for $PC_{61}BM$, D18, PTB7-Th and Y6 films. (b) EQE curves for quasi-tandem narrowband photodetector with different BHJ layer.

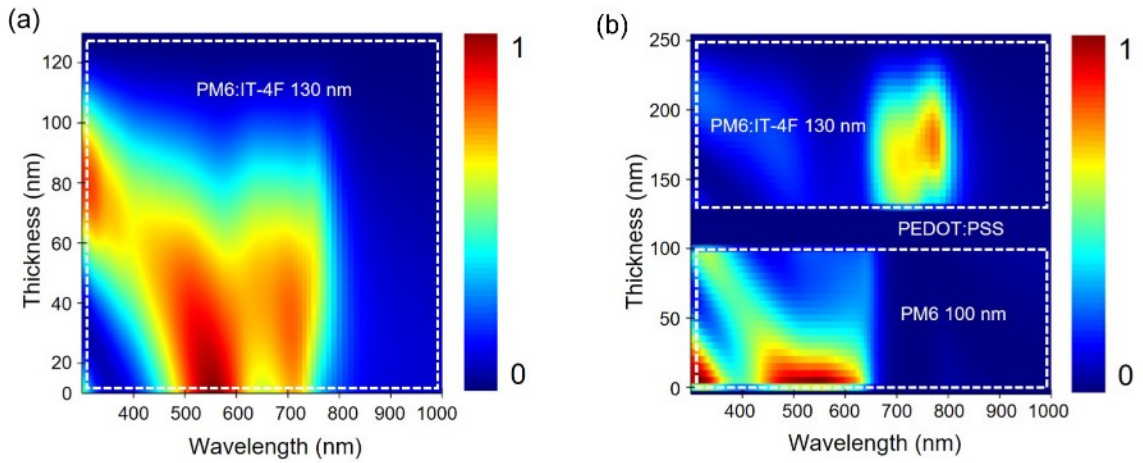

Figure S2. Simulated absorption as the function of film thickness. (a) the PM6:IT-4F BHJ film with thickness of 130nm. (b) the PM6/ PEDOT: PSS/ PM6:IT-4F muti-stack structure with a 100nm thin PM6 layer.

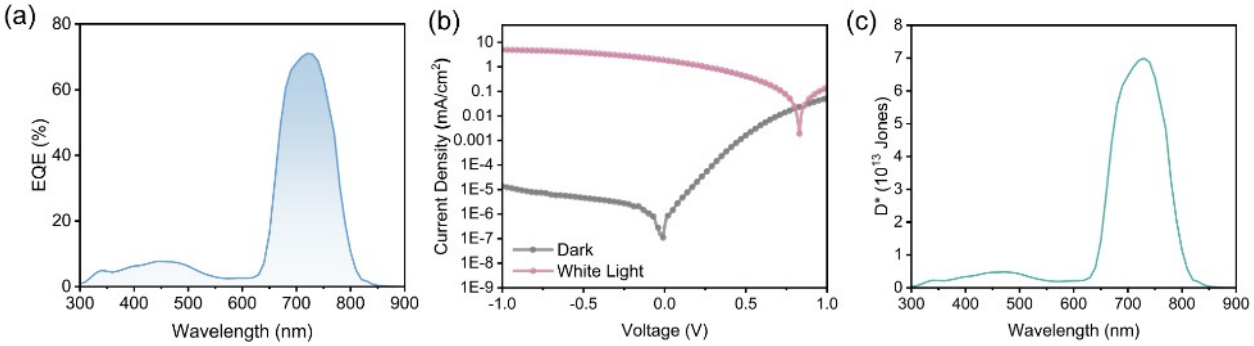

Figure S3. Characteristics of SS-prepared QT-NPDs. (a) EQE curve. (b) dark current and photocurrent. (c) the specific detectivity.

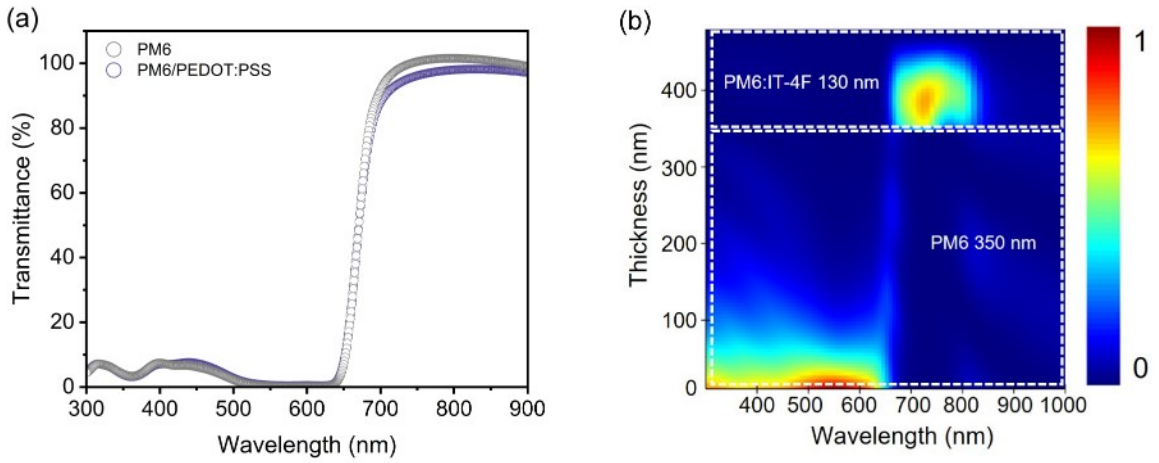

Figure S4. (a) The transmittance curve of PM6 and PM6/ PEDOT:PSS films. (b) Simulated absorption distribution of SS-prepared PM6/PM6:IT-4F heterojunction.

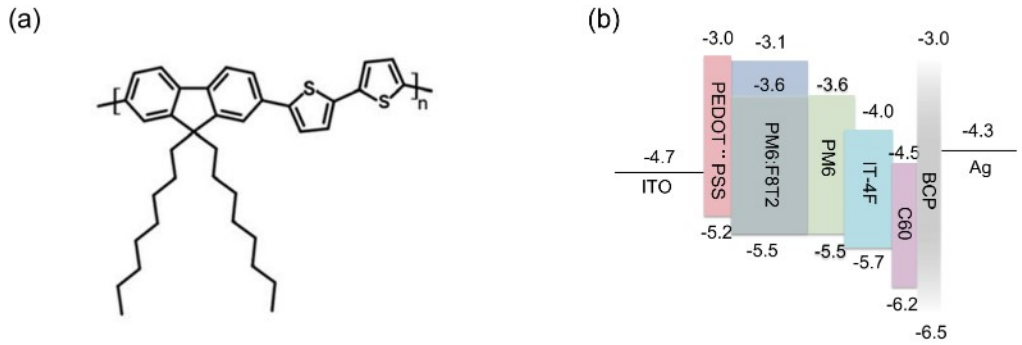

Figure S5. (a) The chemical structures of F8T2. (b) The energy level diagram of the binary-donor blended layer QT-NPDs.

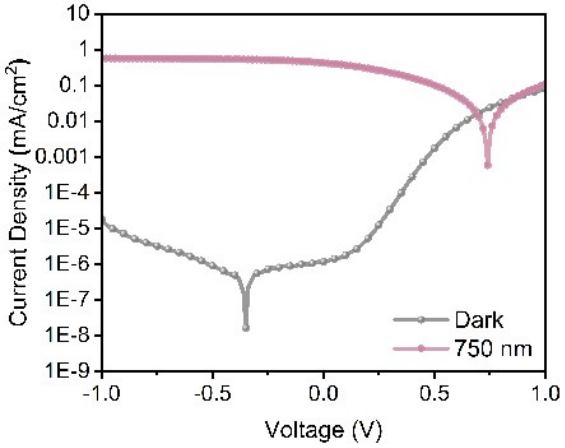

Figure S6. J-V curves of the QT-NPDs with binary-donor blended layer under 750 nm illumination and dark conditions.

Table S1 Summary of parameters for state-of-the-art organic-based narrowband photodetectors.

Architecture	Range (nm)	R_{max}/Peak (A/W)/(nm)	Rise/Fall time(μs)	D* (Jones)	Ref
NT812/Y6	780-950	0.451/860	-	$2.4*10^{12}$	[7]
PM6/Y6	850-950	0.194/892	-	$2.12*10^{13}$	[8]
DPP-DTT:$PC_{70}BM$	900-1000	0.06/940		$>10^{12}$	[9]
PTB7-Th/PTB7-Th:CO8DFC:$PC_{71}BM$	750-1050	0.32/950	6.2/7.0	$>10^{11}$	[10]
PM6:IT-4F/ P3HT/PM6:Y6	750-900	0.5/850	4.3/21	$4.08*10^{12}$	[11]
$MAPbI_3$/CuSCN/PM6:Y6	750-950	0.485/810	39.5/60.8	$8.03*10^{12}$	[12]
$FAMAPbI_3$/PFN-Br/PM6:Y6	780-950	0.55/850 estimated	5.6/6.05	$3*10^{13}$	[13]
$MAPBr_xI_{3-x}$/PFN/PM6: NFA	740-840	0.346/840	0.77/1.15	$5.19*10^{12}$	[14]
$MAPbI_3$/PFN/PM6:Y6	770-900	0.577/850	1.73/0.97	$1.52*10^{13}$	[15]
PM6/PM6:IT-4F	**650-800**	**0.37/730**	**56/40**	**$\sim10^{13}$**	**This work**

Reference：

[1] P. E. Shaw, A. Ruseckas, I.D.W. Samuel., *Advanced Materials.* **2008**, *20*, 3516-3520.
[2] T. Stübinger, W. Brütting, *Journal of Applied Physics.* **2001**, *90*, 3632-3641.
[3] K. Jiang, J. Zhang, Z. Peng, F. Lin, S. Wu, Z. Li, Y. Chen, H. Yan, H. Ade, Z. Zhu, A.K. Jen, *Nature Communications.* **2021**, *12*, 468.
[4] X. Lu, J. Li, Y. Zhang, Z. Han, Z. He, Y. Zou, X. Xu, *Advanced Photonics Research.* **2022**, *3*, 2100335.
[5] W. Jang, H.M. Luong, M.S. Kim, T.Q. Nguyen, D.H. Wang, *Advanced Materials.* **2024**, *36*, 2406316.
[6] M.S. Kim, J. Lim, W. Jang, D.H. Wang, *Advanced Functional Materials.* **2025**, 2422804.
[7] B. Xie, R. Xie, K. Zhang, Q. Yin, Z. Hu, G. Yu, F. Huang, Y. Cao, *Nature Communications.* **2020**, *11*, 2871.
[8] Q. Liu, S. Zeiske, X. Jiang, D. Desta, S. Mertens, S. Gielen, R. Shanivarasanthe, H.-G. Boyen, A. Armin, K. Vandewal, *Nature Communications.* **2022**, *13*, 5194.
[9] A. Armin, R.D. Jansen-van Vuuren, N. Kopidakis, P.L. Burn, P. Meredith, *Nature Communications.* **2015**, *6*, 6343.
[10] Z. Lan, Y.S. Lau, Y. Wang, Z. Xiao, L. Ding, D. Luo, F. Zhu, *Advanced Optical Materials.* **2020**, *8*, 2001388.
[11] M. He, J. Han, L. Guo, X. Han, L. Wei, C. Han, H. Yu, J. Gou, G. Li, D. Lu, Z. Wu, J. Wang, *Advanced Functional Materials.* **2025**, 2504273.
[12] Z. Liu, L. Tao, Y. Zhang, G. Zhou, H. Zhu, Y. Fang, G. Wu, D. Yang, H. Chen, *Advanced Optical Materials.* **2021**, *9*, 2100288.
[13] R. Ollearo, X. Ma, H.B. Akkerman, M. Fattori, M.J. Dyson, A.J.J.M.v. Breemen, S.C.J. Meskers, W. Dijkstra, R.A.J. Janssen, G.H. Gelinck, *Science Advances.* **2023**, *9*, eadf9861.
[14] Y. Zhang, W. Nie, M. Hu, W. Liu, H. Liu, X. Huo, Y. Lu, D. Song, B. Qiao, Z. Liang, Z. Jiao, Z. Xu, G. Yuan, S. Zhao, *ACS Photonics.* **2023**, *10*, 3521-3530.
[15] Y. Zhang, Z. Qin, X. Huo, D. Song, B. Qiao, S. Zhao, *ACS Applied Materials & Interfaces.* **2021**, *13*, 61818-61826.